

Mechanisms of anomalous compressibility of vitreous silicaAlisha N. Clark,^{1,*} Charles E. Leshner,^{1,2} Steven D. Jacobsen,³ and Sabyasachi Sen⁴¹*Department of Earth and Planetary Sciences, University of California, Davis, California 95616, USA*²*Department of Geoscience, Aarhus University, DK-8000 Aarhus C, Denmark*³*Department of Earth and Planetary Sciences, Northwestern University, Evanston, Illinois 60208, USA*⁴*Department of Materials Science, University of California, Davis, California 95616, USA*

(Received 2 May 2014; revised manuscript received 22 October 2014; published 20 November 2014)

The anomalous compressibility of vitreous silica has been known for nearly a century, but the mechanisms responsible for it remain poorly understood. Using GHz-ultrasonic interferometry, we measured longitudinal and transverse acoustic wave travel times at pressures up to 5 GPa in vitreous silica with fictive temperatures (T_f) ranging between 985 °C and 1500 °C. The maximum in ultrasonic wave travel times—corresponding to a minimum in acoustic velocities—shifts to higher pressure with increasing T_f for both acoustic waves, with complete reversibility below 5 GPa. These relationships reflect polyamorphism in the supercooled liquid, which results in a glassy state possessing different proportions of domains of high- and low-density amorphous phases (HDA and LDA, respectively). The relative proportion of HDA and LDA is set at T_f and remains fixed on compression below the permanent densification pressure. The bulk material exhibits compression behavior systematically dependent on synthesis conditions that arise from the presence of floppy modes in a mixture of HDA and LDA domains.

DOI: [10.1103/PhysRevB.90.174110](https://doi.org/10.1103/PhysRevB.90.174110)

PACS number(s): 64.70.ph, 61.25.-f, 61.43.Fs, 62.50.-p

I. INTRODUCTION

The structure of vitreous silica ($v\text{-SiO}_2$) consists of a fully polymerized, continuous random network of corner-sharing SiO_4 tetrahedra that becomes softer, rather than stiffer, when compressed. The anomalous compressibility behavior persists on hydrostatic loading up to 2–3 GPa at room temperature [1–4]. Bridgman and subsequent workers demonstrated that the deformation of the network is fully reversible below the onset of permanent densification at ~ 8 GPa [2–5]. It is also well known that the longitudinal and transverse acoustic wave velocities for $v\text{-SiO}_2$ decrease with increasing pressure up to ~ 2.5 GPa, consistent with the anomalous compressibility found in this pressure range [6–11].

Bridgman [2] posited that $v\text{-SiO}_2$ softens on compression because of its relatively open network structure and the manner of collapse on compression. Permanent densification at high pressures and temperatures is accommodated by changes in ring structures and Si coordination number [12,13]. Below the onset of permanent densification, these structural rearrangements are not active, and the rotation of the SiO_4 tetrahedra is proposed to be the active densification mechanism. However, the origin of anomalous compressibility in $v\text{-SiO}_2$ remains controversial, with contrasting models of tetrahedral rotation advanced in the literature.

Vukceвич [14] and others [15–17] proposed a two-state structural model whereby $v\text{-SiO}_2$ transforms from a low-density amorphous phase to a high-density amorphous phase (LDA and HDA, respectively), i.e., polyamorphic phase transition, with increasing pressure or temperature, analogous to the α - β transition in crystalline silica. The displacive α - β phase transition in cristobalite is accommodated by the tetrahedral rotation of six-member rings. The β phase (low-density polymorph) has more symmetric intertetrahedral

bonding than the α phase (high-density polymorph) making it stiffer, resulting in a higher bulk modulus (K). If LDA (β -like) and HDA (α -like) phases possess analogous properties to the cristobalite polymorphs as proposed by the two-state model, the compressibility of $v\text{-SiO}_2$ should depend on their relative stability and, if both are stable due to spinodal decomposition, then by their relative abundance [16,17]. Below and above the spinodal region, $v\text{-SiO}_2$ should behave normally, governed by K for LDA and HDA, respectively, whereas within the two-phase region the conversion of LDA domains to HDA domains with increasing pressure will lead to softening of the bulk material. In this model, the pressure interval of anomalous compressibility reflects the limits of the coexistence of LDA and HDA.

Experimental evidence for a spinodal in $v\text{-SiO}_2$ comes from the unusual T - ρ relations at low pressure. Dilatometric and spectroscopic data show that density increases anomalously between ~ 950 °C and at least up to 1500 °C, whereas density decreases with temperature for liquid SiO_2 above ~ 1935 °C [18–21]. These relationships imply an underlying phase transition extending over a finite temperature interval with a negative Clapeyron slope, where the low-temperature LDA phase is stable below the spinodal and the high-temperature HDA phase is stable above it [21].

An alternative model, the flexibility hypothesis advanced by Dove and co-workers [22–24] among others, calls on a purely dynamic response to compression to explain the anomalous compressibility of $v\text{-SiO}_2$ involving low-energy deformation by rotation of rigid SiO_4 tetrahedral units freely hinged to coordinated tetrahedra giving rise to so-called floppy modes. Mode softening results from the weakening of the network as the undeformed SiO_4 tetrahedra dynamically rotate during compression. As the network buckles, the material softens until short-range repulsive forces impede further collapse of structural voids [25]. The network flexibility model accounts for anomalous compressibility; however, it does not readily explain the increase in density with temperatures found on

*Corresponding author: anclark@ucdavis.edu

heating v -SiO₂ at 1 atm. It also needs emphasizing that polymorphism and floppy modes are not mutually exclusive [15,22], but establishing their relative importance in densification of v -SiO₂ remains a challenging yet fundamental step towards further understanding deformation of amorphous materials composed of open tetrahedral networks.

In this study we examined ultrasonic wave propagation in v -SiO₂ during compression at room temperature for samples synthesized at 1 atm but quenched from different temperatures between the density minimum at ~ 950 °C and maximum at ~ 1935 °C. Fictive temperatures (T_f) of these samples range from 985 °C to 1500 °C, corresponding to a density increase of $\sim 0.3\%$. We predict that if both LDA and HDA domains with different compressibility coexist and their relative abundance is a function of temperature, then glasses with different T_f will return to normal behavior at different pressures. In contrast, if the anomalous compressibility is due to floppy rotational modes in a single phase, then either the compressibility behavior will be independent of T_f , or v -SiO₂ with a higher initial density (i.e., higher T_f) will reach rotational lockup and return to normal behavior at lower pressures.

II. EXPERIMENTAL METHODS

Three high-purity v -SiO₂ samples with different T_f were synthesized at Corning Inc. The samples were prepared by chemical vapor deposition and annealed at 985 °C, 1300 °C, and 1550 °C for 1500, 4, and 0.5 hours, respectively, followed by quenching in air [21]. Fourier transform infrared (FTIR) spectra were collected using a Bruker TENSOR 37 FTIR spectrophotograph and HYPERION microscope with high-sensitivity

MCT detector. We used a 15-mm pixel size detector in conjunction with $15\times$ all-reflecting IR objective. Data were collected at 1 cm^{-1} resolution and 256 scans. T_f of these samples was determined from the position of the $\sim 2260\text{ cm}^{-1}$ overtone band in the infrared absorption spectra with $T_f \sim 985$ °C, 1260 °C, and 1500 °C, respectively, for the three samples listed above (see [26], and Supplemental Material [27]). The densities of the samples at ambient pressure were determined by Archimedes' method and are reported together with other material properties in Table I.

We used GHz-ultrasonic interferometry in a diamond anvil cell to measure the travel times of acoustic longitudinal (P) and transverse (S) wave tone bursts through the three v -SiO₂ samples as a function of hydrostatic pressure (Fig. 1). The 1-atm P - and S -wave velocities for all three v -SiO₂ samples were determined using ~ 1 -mm double-polished plates. Samples for high-pressure measurements were 150- μm -diameter disks cored from a double-polished thin section $\sim 50\text{ }\mu\text{m}$ thick. Gigahertz P -wave transducers consisted of ZnO thin films ($\sim 1.5\text{ }\mu\text{m}$ thickness) sputtered onto single-crystal sapphire buffer rods. The buffer rods are mechanically coupled to the polished-plate sample for the 1-atm measurements and to the diamond anvil in contact with the sample for the high-pressure measurements. For S -wave buffer rods we used a single-crystal yttrium aluminum garnet (YAG) prism wherein a P - to S -wave conversion takes place before entering the sample for 1-atm measurements or the diamond anvil for high-pressure measurements. We first measured the travel time of the high-pressure samples on the culet of the open diamond anvil cell to determine the initial travel time (t_0). The cell was loaded with a ruby pressure marker [28] and

TABLE I. Physicochemical characteristics of v -SiO₂ samples used in this study at ambient conditions.

	v -SiO ₂ sample A	v -SiO ₂ sample B	v -SiO ₂ sample C
Density (g cm^{-3}) ^a	2.199 ± 0.002	2.203 ± 0.002	2.207 ± 0.002
OH content (ppm) ^b	268 ± 7	79 ± 4	244 ± 5
T_f (deg C) ^c	985 ± 20	1260 ± 30	1500 ± 40
V_P (m/s) ^{d,e}	5902 ± 1.0	5944 ± 1.0	5977 ± 0.9
V_S (m/s) ^{d,e}	3765 ± 0.6	3757 ± 0.6	3751 ± 0.6
K (GPa) ^{d,f}	35.0 ± 0.15	36.4 ± 0.15	37.4 ± 0.15
G (GPa) ^{d,g}	31.2 ± 0.04	31.1 ± 0.04	31.1 ± 0.04
P -wave linear fit (Positive limb)	$y = 0.0737x + 1.0019$ $R^2 = 0.99263$	$y = 0.0656x + 1.0104$ $R^2 = 0.9887$	$y = 0.0563x + 1.024$ $R^2 = 0.98821$
P -wave linear fit (Negative limb)	$y = -0.037x + 1.2144$ $R^2 = 0.99218$	$y = -0.0335x + 1.2257$ $R^2 = 0.99133$	$y = -0.0324x + 1.2193$ $R^2 = 0.99355$
Intersection (GPa)	1.92	2.17	2.20
S -wave linear fit (Positive limb)	$y = 0.0646x + 1.0003$ $R^2 = 0.99556$	$y = 0.0571x + 0.9947$ $R^2 = 0.99349$	$y = 0.0548x + 1.0077$ $R^2 = 0.99279$
S -wave linear fit (Negative limb)	$y = -0.0187x + 1.1707$ $R^2 = 0.99098$	$y = -0.0182x + 1.1752$ $R^2 = 0.98226$	$y = -0.0157x + 1.1762$ $R^2 = 0.97513$
Intersection (GPa)	2.05	2.35	2.39

^aMeasured by Archimedes' method.

^bMeasured by FTIR spectroscopy and calculated by the method of [32]. See Appendix A in the Supplemental Material [27].

^cMeasured by FTIR spectroscopy and calculated by the method of [26]. See Appendix A in the Supplemental Material [27].

^d V_P , V_S , K , and G correspond to P - and S -wave velocities and bulk and shear moduli, respectively. See Appendix B in the Supplemental Material for details and data tables [27].

^e $V = \frac{2L}{t}$.

^f $K_S = \rho (V_P^2 - \frac{4}{3}V_S^2)$.

^g $G = \rho V_S^2$.

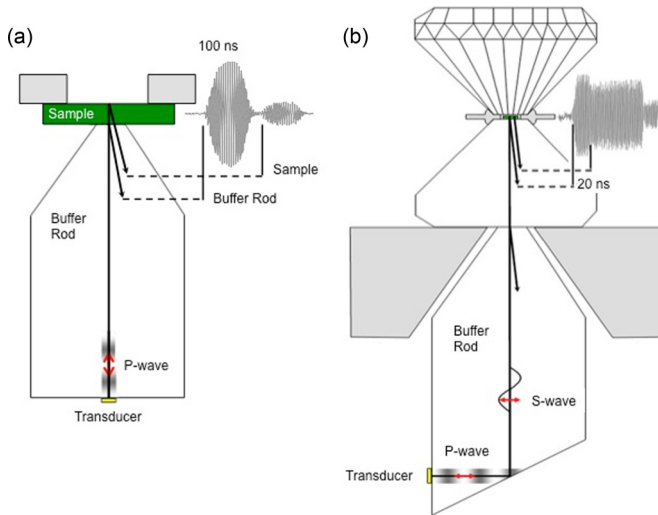


FIG. 1. (Color online) Schematic diagrams of the GHz-frequency-ultrasonic interferometry experimental setup. (a) The P -wave buffer rod coupled directly to a sample at 1 atm. The 100-ns GHz-frequency wave packet is produced by the GHz-frequency P -wave transducer located at the base of the Al_2O_3 buffer rod. The wave packets are reflected from the buffer rod-sample interface, and the far side of the sample. Travel time is calculated from the interference of these two echoes. (b) Production of the S wave from the incident P wave in the high-pressure DAC assembly. Here the GHz-frequency P -wave transducer is mounted on the side of the YAG buffer rod. The wave packet is converted from P to S waves by exploiting Snell's law at a precisely oriented face at the base of the buffer rod. The wave packet travels up the buffer rod, through the diamond, and into the sample (which is mounted flush to the diamond culet). At each interface a portion of the wave is transmitted and reflected. For high-pressure measurements the signals interfered to calculate travel time are reflected from the diamond-sample interface, and the far side of the sample. The interfered signal shown here is 100 ns with the sample signal appearing 20 ns after the diamond culet signal. Modified from [30].

a 16:3:1 mixture of methanol:ethanol:water which served as the hydrostatic pressure medium [29]. Tone bursts of the GHz-frequency carrier signal reflected from the near and far side of the polished glass sample were interfered in time by varying the tone burst duration (Fig. 2). The frequency was scanned at 0.5-MHz frequency steps from 0.7 to 1.7 GHz to produce an acoustic interferogram. The round-trip travel times are determined from the frequency spacing of maxima and minima of the interferogram (Fig. 3). The resulting travel times are determined with a precision of one part in 10^3 (about ± 0.02 ns out of 20 ns). Further details of the associated experimental methodology can be found elsewhere [30].

III. RESULTS AND DISCUSSION

We measured ultrasonic wave travel times at ~ 0.25 GPa pressure steps from 0 to 5 GPa. P - and S -wave measurements were carried out separately. In several experiments, travel times were also collected on decompression to test for reversibility (Fig. 4 and Appendix C in the Supplemental Material [27]). After each pressure adjustment, data were

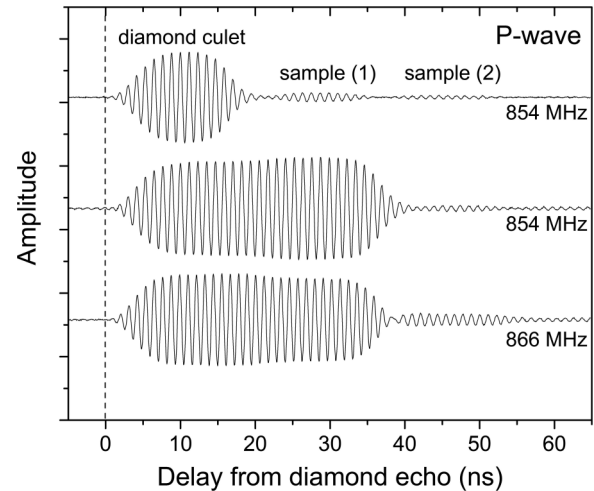


FIG. 2. P -wave echoes of sample $T_f = 985^\circ\text{C}$ at 0.11 ± 0.05 GPa (985_P1_61). (Top) 20-ns echoes from the diamond culet-sample boundary with two sample echoes (far side of the sample) at 854 MHz frequency. (Middle) 40-ns diamond culet signal interfered with the sample echo (at ~ 25 – 35 ns) at 854 MHz frequency. There is positive interference with the sample and diamond echoes at this frequency corresponding to a maximum in the interferogram. (Bottom) 40-ns diamond culet signal interfered with the sample echo (at ~ 25 – 35 ns) at 866 MHz frequency. There is negative interference with the sample and diamond echoes at this frequency corresponding to a minimum in the interferogram.

collected every 10 min with a minimum of 1 h between pressure adjustments to evaluate any time dependence of the travel time measurements. P -wave data for the 985°C T_f sample includes two compression-decompression cycles (0–4.5 GPa) performed without reloading the sample. P - and S -wave travel times were normalized to the 1-atm travel time (t_0) and plotted in Fig. 4. Within uncertainties, the normalized travel times for a given pressure and T_f sample are identical for the compression and decompression paths of a given run, and among replicate experiments.

As shown in Fig. 4, the travel times for both P and S waves increase with pressure up to 2–3 GPa, regardless of T_f . Moreover, this behavior occurs despite the increase in sample density and reduction in sample length, requiring that over this pressure range the compressibility increases with pressure at GHz frequencies, as has been shown previously at MHz frequencies [7,11]. Since we lack direct measurements of sample length and density along our compression/decompression paths, we cannot calculate P - and S -wave velocities, and elastic parameters; however, the normalized travel time curves do constrain the transition from anomalous to normal compression behavior. P -wave travel times reach maximum values near 2.0, 2.2, and 2.4 GPa for 985°C , 1260°C , 1500°C T_f samples, respectively, corresponding to a 12%–13% increase in travel time relative to the 1-atm values (Fig. 4). Normalized S -wave travel times exhibit a similar increase with T_f over this pressure range, although the maximum in travel times occurs ~ 0.3 GPa higher in pressure for each sample.

We employed two methods to constrain the pressure at which the pressure dependence of the travel time changes from

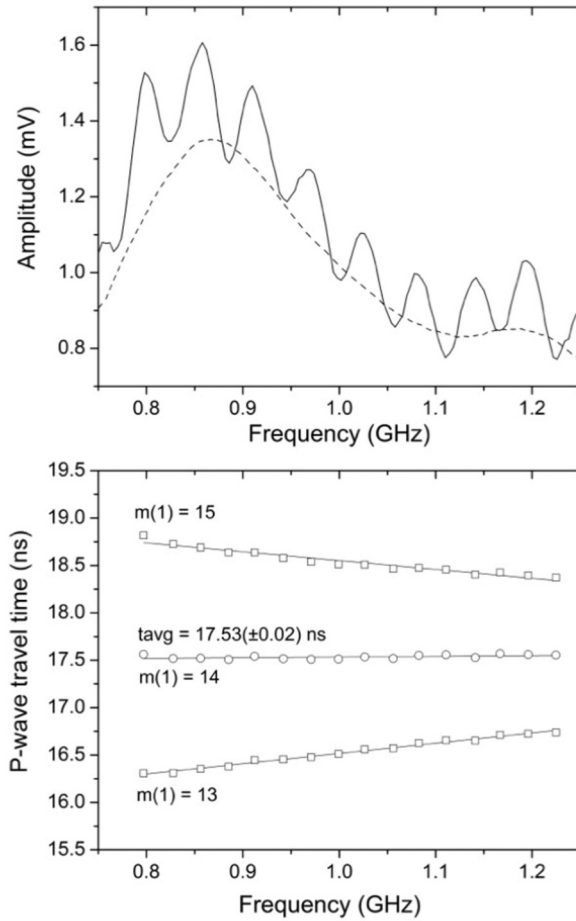


FIG. 3. (Top) Interferogram sample $T_f = 985^\circ\text{C}$ at 0.11 ± 0.05 GPa (985_P1_61) from 0.75 to 1.25 GHz. The dashed curve is the amplitude of the diamond culet signal and the solid curve is the interfered diamond culet–sample signal (see Fig. 2.) Spacing between two maxima corresponds to an integer number of wavelengths in the sample. (Bottom) Calculated travel time as a function of frequency from 0.75 to 1.25 GHz from the above interferogram. The number of wavelengths in the sample is indicated by the m value. Incorrect m values result in frequency-dependent travel times [e.g., $m(1) = 13$ and 15]. Travel time is determined from the m value that provides frequency-independent measurements [e.g., $m(1) = 14$].

positive to negative. The first method assigns the pressure of the maximum along the t/t_0 curve (dashed line in Fig. 4) as the transition pressure. This works well when there are sufficient data covering the 2–3 GPa pressure interval. The second method computes the intersection of extrapolated linear best fits to the positive (anomalous) and negative (normal) limbs of the normalized travel time curves (see Appendix C in the Supplemental Material [27]). The results are summarized in Table I and the bounds on the transition from anomalous to normal behavior are shown on Fig. 4 as the crosshatched polygons.

Regardless of the method used to determine the location of the maximum in the t/t_0 curve, the pressure of the transition from anomalous to normal behavior shifts to higher values with increasing T_f or initial density of $v\text{-SiO}_2$ (Fig. 5). This is not expected if the anomalous compressibility is solely due to the collapse of the rigid tetrahedral network

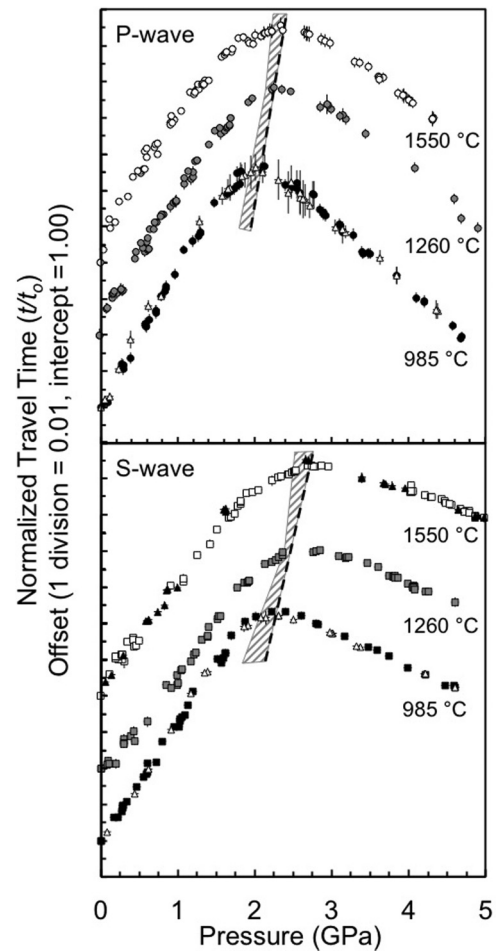


FIG. 4. P - and S -wave travel time curves normalized to the 1-atm travel time shown as circles and squares, respectively. The normalized travel time scale is offset. The intercept is $t/t_0 = 1.00$, with one division = 0.01. Black, gray, and white circles (P wave) and squares (S wave) correspond to $T_f = 985^\circ\text{C}$, 1260°C , and 1550°C data sets, respectively. Decompression data are shown as triangles in contrasting colors for both P - and S -wave travel time curves (i.e., white and black for $T_f = 985^\circ\text{C}$ and 1550°C , respectively). The dashed line is to guide the eye to the location of the maximum t/t_0 measurement. The gray box bounds the pressure region between the maximum travel time location, and the pressure calculated as the intersection of the extrapolated positive (anomalous) and negative (normal) limbs of the travel time curves (see text for discussion, and Appendix C in the Supplemental Material [27] for further details and data tables).

postulated for the flexibility (floppy mode) hypothesis, where the return to normal behavior should occur once the volume reduction reaches the atomic repulsion limit. That is, the $v\text{-SiO}_2$ sample with the higher initial density should reach this locking limit at lower pressure as the atoms are in closest proximity before compression. On the other hand, anomalous compressibility cannot be the consequence of changes in the proportion of LDA and HDA with pressure as proposed by proponents of polyamorphism. Firstly, we observe no time dependence or hysteresis in the t/t_0 curves during compression and decompression—even following multiple compression–decompression cycles—as would be expected if the time scale

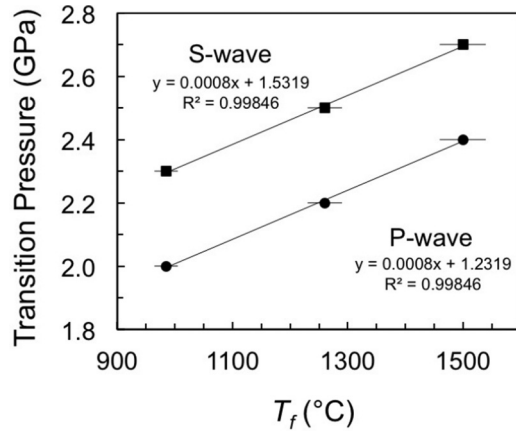


FIG. 5. Pressure associated with the maximum t/t_o indicating the transition from anomalous to normal behavior for P - and S -wave data sets as a function of T_f are shown as closed circles and squares, respectively. Linear fits to the maximum pressure associated with the maxima in t/t_o data are also shown.

for phase transitions and/or structural relaxation are less than or equal to the observational time scale. Secondly, given that our study was carried out on glasses having different initial bulk properties, if LDA is to convert to HDA on compression at room temperature one expects the two-way travel time curves to converge at high pressure—which is not observed at least up to 4.7 GPa. In summary, the reproducibility and reversibility of t/t_o curves coupled with differences related to T_f imply that the proportion of LDA and HDA in a given sample remains constant during room temperature compression and decompression. While the anomalous elastic behavior of v -SiO₂ presented here requires the presence of both LDA and HDA, it cannot arise from an active transition between the two amorphous states.

The exact proportions of LDA and HDA in our samples is not known, but the 1-atm T - ρ relations reflecting a negative Claperyon slope for the LDA-HDA spinodal field [21] provides guidance. The sample with a T_f of 985 °C reflects annealing close to the density minimum and thus possesses the greatest amount of LDA, while the sample with a T_f of 1500 °C and annealed closer to the high-temperature density maximum has the least amount of LDA. We estimate that the sample with a T_f of 1260 °C lying about halfway between the extrema in density has subequal proportions of HDA and LDA. Although the precise volumetric proportions of LDA and HDA in our samples are not known, importantly there is a systematic shift in the location of the maximum in the t/t_o curves to higher pressure with increasing T_f (Figs. 4 and 5). This implies that the return to normal behavior shifts to higher pressure as the initial proportion of HDA increases. This interdependence of T_f , abundance of LDA and HDA, and pressure at which v -SiO₂ reverts to normal (decreasing) two-way travel times with increasing pressure provides persuasive evidence that LDA is more compressible than HDA. That is, LDA being initially less dense than HDA must reach a locking limit at lower pressure. Supporting this interpretation is the positive dependence of the 1-atm bulk modulus (K_S) on T_f (density and proportion of HDA) shown in Fig. 6. The near constancy of

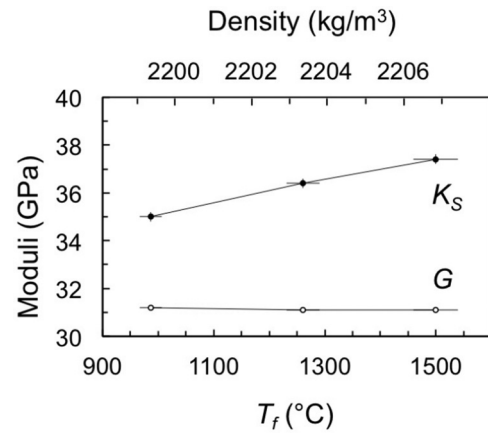


FIG. 6. Bulk (K_S) and shear (G) moduli as a function of T_f shown as closed and open circles, respectively. K_S increases as density (and T_f) increase. G is near constant over the T_f range explored in this study. Errors shown are reported in Table I and for G are smaller than the symbol (see Appendix B in the Supplemental Material [27]).

G (~ 31 GPa) may largely be fortuitous reflecting an offsetting effect of differences in the abundance and shear moduli for LDA and HDA.

We propose that the observed T_f - t/t_o relationships reflect network flexibility within a two-phase mixture that have fixed proportions up to at least 5 GPa, with normal behavior occurring upon the collapse of the network to a critical density where the repulsive atomic forces dominate energetically over tetrahedral rotation. The fact that all the samples exhibit the same magnitude of increase in the t/t_o curves requires that the mechanism underlying the anomalous behavior is active in both LDA and HDA phases—the differences we show here with T_f simply reflect the relative abundance of the two phases and their respective K_S . If the proposed mechanism was active only in one phase, the magnitude of the increase in the t/t_o curve should be dependent on the proportion of phases present in the sample, which is not observed in our data. This does not imply that the LDA and HDA phases have the same topology, but that the manner of network collapse is similar in both phases. LDA (low K_S) and HDA (high K_S) phases both show anomalous behavior on compression, in direct contrast to the polyamorphism model, which predicts that both the LDA and HDA behave normally on compression and that it is the transition from the low-compressibility LDA to the higher-compressibility HDA that leads to the anomalous behavior.

IV. CONCLUSION

In summary, the results presented here provide evidence for polyamorphism in liquid silica that upon quenching results in glasses with frozen-in LDA and HDA phase assemblages. The relative volumetric proportions of these phases depend on the thermal history of the glass with the fraction of the HDA increasing with T_f . Regardless of T_f , v -SiO₂ shows anomalous compressibility between 0 and ~ 3 GPa, consistent with previous studies; however, this work shows in detail that the elastic properties of v -SiO₂ vary systematically with T_f , i.e., the proportions of LDA and HDA. We attribute the

anomalous compressibility to floppy mode tetrahedral rotation, i.e., the flexibility hypothesis, but in a two-phase mixture, consistent with the proposed structural differences between HDA and LDA phases. The difference in bulk compressibility among glasses with different T_f is consequently explained by the relative fraction of these phases. The observed behavior requires that LDA is more compressible than HDA in order for LDA to reach the repulsive limit and return to normal behavior at lower pressure. Thus, both floppy modes and the coexistence of varying fractions of HDA and LDA phases are critical factors controlling the elastic properties of v -SiO₂, and may be the underlying cause of anomalous compressibility found in other network glasses and melts [11,31].

ACKNOWLEDGMENTS

A.N.C. and C.E.L. were supported by NSF Grant No. 318 EAR 1215714 and University of California Grant No. UCLAB 09-LR-03-227404-LESC. C.E.L. also acknowledges support from the Danish National Research Foundation. S.D.J. acknowledges support from NSF Grant No. EAR-0748707, the Carnegie/DOE Alliance Center (CDAC), the David and Lucile Packard Foundation, and the Alexander von Humboldt Foundation. S.S. was supported by NSF Grant No. DMR 1104869. We thank Yun-Yuan Chang, John Lazarz, and Laurel Childress for assistance with experiments. We acknowledge four anonymous reviewers for comments that helped to improve this manuscript.

-
- [1] P. W. Bridgman, *Am. J. Sci.* **10**, 359 (1925).
 [2] P. W. Bridgman, *Am. J. Sci.* **237**, 7 (1938).
 [3] C. Meade and R. Jeanloz, *Phys. Rev. B* **35**, 236 (1987).
 [4] O. B. Tsiok, V. V. Brazhkin, A. G. Lyapin, and L. G. Khvostantsev, *Phys. Rev. Lett.* **80**, 999 (1998).
 [5] P. W. Bridgman, *Proc. Am. Acad. Arts Sci.* **76**, 71 (1948).
 [6] E. H. Bogardus, *J. Appl. Phys.* **36**, 2504 (1965).
 [7] K. Kondo, S. Lio, and A. Sawaoka, *J. Appl. Phys.* **52**, 2826 (1981).
 [8] J. Schroeder, T. G. Bilodeau, and X. Zhao, *High Press. Res.* **4**, 531 (1990).
 [9] C. S. Zha, R. J. Hemley, H. K. Mao, T. S. Duffy, and C. Meade, *Phys. Rev. B* **50**, 13105 (1994).
 [10] M. Grimsditch, *Phys. Rev. Lett.* **52**, 2379 (1984).
 [11] K. Suito, M. Miyoshi, T. Sasakura, and H. Fujisawa, in *High-Pressure Research: Application to Earth and Planetary Science*, edited by Y. Sayano and M. H. Manghnani (American Geophysical Union, Washington, DC, 1992), pp. 219–225.
 [12] L. P. Dávila, M. J. Caturla, A. Kubota, B. Sadigh, T. Díaz de la Rubia, J. F. Shackelford, S. H. Risbud, and S. H. Garofalini, *Phys. Rev. Lett.* **91**, 205501 (2003).
 [13] B. B. Karki, D. Bhattarai, and L. Stixrude, *Phys. Rev. B* **76**, 104205 (2007).
 [14] M. R. Vukcevic, *J. Non-Cryst. Solids* **11**, 25 (1972).
 [15] L. P. Huang, L. Duffrene, and J. Kieffer, *J. Non-Cryst. Solids* **349**, 1 (2004).
 [16] L. Huang and J. Kieffer, *Phys. Rev. B* **69**, 224204 (2004).
 [17] D. J. Lacks, *Phys. Rev. Lett.* **84**, 4629 (2000).
 [18] J. F. Bacon, A. A. Hasapis, and J. W. Wholley, Jr., *Phys. Chem. Glasses* **1**, 90 (1960).
 [19] R. Brückner, *J. Non-Cryst. Solids* **5**, 123 (1970).
 [20] H. Kakiuchida, K. Saito, and A. J. Ikushima, *J. Appl. Phys.* **93**, 777 (2003).
 [21] S. Sen, R. L. Andrus, D. E. Baker, and M. T. Murtagh, *Phys. Rev. Lett.* **93**, 125902 (2004).
 [22] A. M. Walker, L. A. Sullivan, K. Trachenko, R. P. Bruin, T. O. H. White, M. T. Dove, R. P. Tyer, I. T. Todorov, and S. A. Wells, *J. Phys.: Condens. Matter* **19**, 9 (2007).
 [23] K. Trachenko and M. T. Dove, *J. Phys.: Condens. Matter* **14**, 7449 (2002).
 [24] K. Trachenko and M. T. Dove, *Phys. Rev. B* **67**, 064107 (2003).
 [25] M. T. Dove, *Am. Mineral.* **82**, 213 (1997).
 [26] A. Agarwal, K. M. Davis, and M. Tomozawa, *J. Non-Cryst Solids* **185**, 191 (1995).
 [27] See Supplemental Material at <http://link.aps.org/supplemental/10.1103/PhysRevB.90.174110> for FTIR spectra and GHz-ultrasonic data tables.
 [28] H. K. Mao, J. Xu, and P. M. Bell, *J. Geophys. Res.: Solid Earth* **91**, 4673 (1986).
 [29] R. J. Angel, M. Bujak, J. Zhao, G. D. Gatta, and S. D. Jacobsen, *J. Appl. Crystallogr.* **40**, 26 (2007).
 [30] S. D. Jacobsen, H. J. Reichmann, A. Kantor, and H. A. Spetzler, in *Advances in High-Pressure Technology for Geophysical Applications*, edited by J. Chen, Y. Wang, T. S. Duffy, G. Shen, and L. F. Dobrzhinetskaya (Elsevier, Amsterdam, 2005), p. 25.
 [31] T. Sakamaki, A. Suzuki, E. Ohtani, H. Terasaki, S. Urakawa, Y. Katayama, K.-i. Funakoshi, Y. Wang, J. W. Hernlund, and M. D. Ballmer, *Nat. Geosci.* **6**, 1041 (2013).
 [32] E. Stolper, *Contrib. Mineral. Petrol.* **81**, 1 (1982).